NEUTRONIC MODELING AND THERMAL NEUTRON FLUX MEASUREMENT OF THE MCR6 ROD IN THE NRU REACTOR

X. Wang, T.C. Leung
Atomic Energy of Canada Limited, Chalk River Laboratories,
Chalk River, Ontario, Canada, K0J 1P0

Abstract

The six-barrel Multiple-Capsule Water Cooled Rods (MCR6) in the NRU reactor have been used to produce isotopes such as I-131 and Ir-192. This paper describes the modeling of the MCR6 rods and the simulation method used to predict the neutron fluxes. The sensitivity of various radioisotope loadings of MCR6 rods upon flux and power perturbations of neighbouring rods is investigated. This paper also presents the results of thermal neutron flux measurements in one of the MCR6 rods from gold wire detectors using the neutron activation technique. The measured fluxes match very well with the simulated fluxes, within $\pm$ 2%.

1. Introduction

The Nuclear Research Universal (NRU) reactor at the Chalk River Laboratories is a heavy-water cooled and moderated research reactor, with on-line refuelling capability. It is mainly used to produce neutrons for fundamental research, for radioisotope production, and for reactor material and fuel bundle testing. It has a design peak thermal flux of 4.0×10^{14} $n.cm^{-2}.s^{-1}$, and it is licensed to operate at a maximum power of 135 MW [1]. The hexagonal lattice pitch between adjacent rod assemblies is 19.685 cm.

The two six-barrel Multi-Capsule Water Cooled Rods (MCR6) in the NRU reactor have been used to produce radioisotopes such as I-131 and Ir-192. The MCR6 rods were modeled using the computer codes WIMS-AECL (the Winfrith Improved Multi-group Scheme) [2] and TRIAD3 (TRIAngular-Discontinuity-factor-3-dimensional) [3]. The effect of the various loadings of the radioisotopes in MCR6 rods on the calculation results has been assessed. Also, to support ACR-1000 fuel development and design [4], non-fissionable Zirconia Burnable Neutron Absorber (Zr-BNA) material samples were irradiated in an MCR6 rod in the NRU reactor. The thermal neutron fluxes in the Zr-Yttria material samples were measured, which were used in comparing with the simulations.

The purpose of this work is to test the simulation results from WIMS-AECL and TRIAD3 against measurement data of the MCR6 rod. This paper describes the modeling of the MCR6 rods, and presents simulation results for the MCR6 rods with various radioisotope loadings. It also presents the results of the thermal neutron flux measurements from gold wire detectors, and the comparisons between measured and simulated results.

2. Modeling of the MCR6 rod

The NRU reactor consists of different types of rods, such as driver fuel rods, fast-neutron rods, MCR6 rods, Mo-99 production rods, loop fuel strings for bundle testing, absorber rods and control rods. Each of these rods was modeled as 18 axially stacked hexagonal cells, each

of which has uniform neutronic properties. The detailed flux shape and neutron spectrum within each cell are determined by the WIMS-AECL code. The version of WIMS-AECL used in this study is version 2-5d coupled with nuclear data library ENDF/B-V. The uniform neutronic properties for each cell, represented by homogenized cell parameters in two energy groups, are then calculated by weighting (by flux and volume) the region material properties calculated from WIMS-AECL. The homogeneous cell parameters for the hexagonal cells of each rod in the NRU reactor are inputs to the reactor simulation code, TRIAD3 [4], which is used to calculate the flux and power distributions in the NRU core.

2.1 WIMS-AECL models for an MCR6 rod

Figure 1 shows an MCR6 rod assembly, which consists of a cluster of six flow tubes. Each flow tube houses a stringer containing radioisotope capsules. The MCR6 rod is divided into four axial sections: top section, capsule section, spacer section, and bottom section. The top section consists of six aluminum flow tubes, inside which aluminum stringer tubes are filled with D_2O. In the capsule and spacer section, aluminum capsules of about 8 cm long each are stacked on one another in the middle of each stringer with spacers on both the top and the bottom. The number of the capsules varies from about 6 to 20 per stringer depending on the required loading. Radioisotope samples are put in the capsules in the forms of slugs or pellets. The bottom section is an aluminum rod with six evenly distributed holes filled with D_2O.

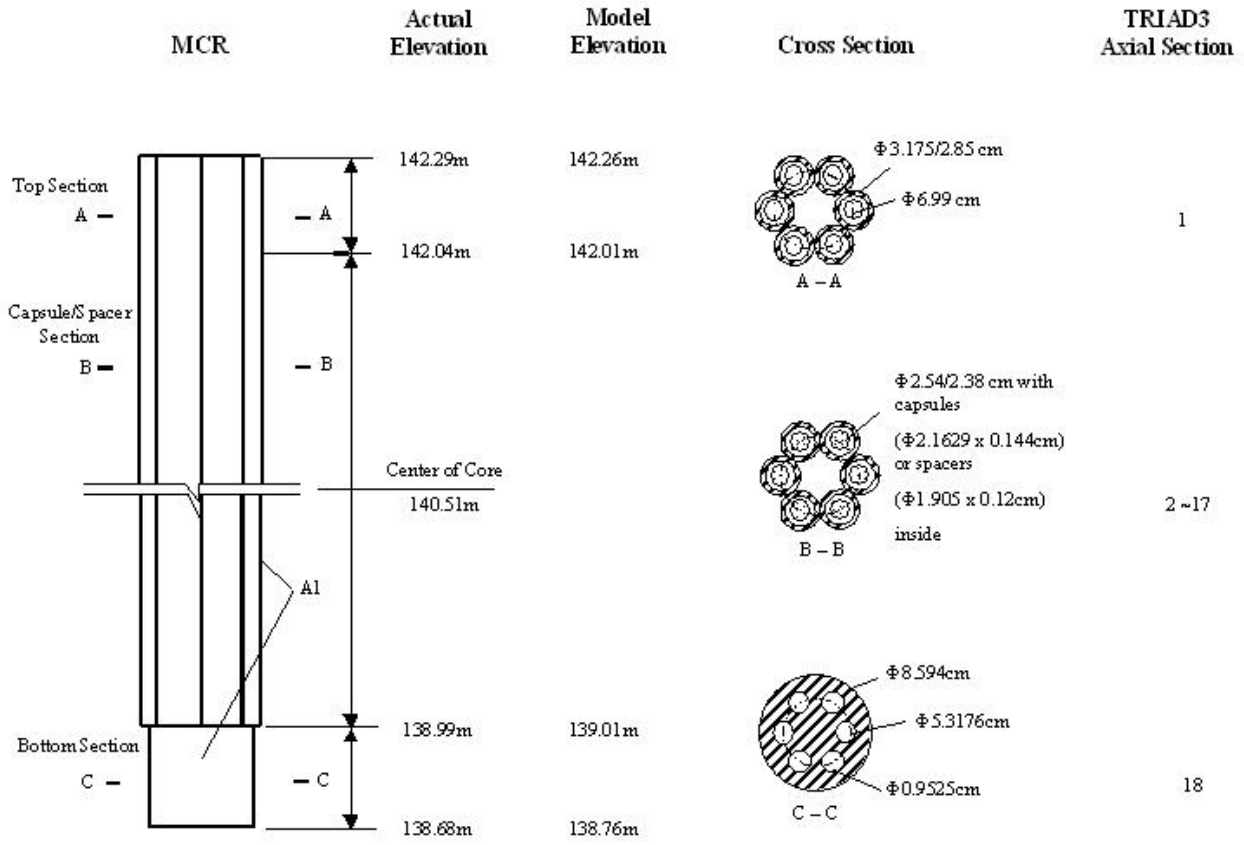

Figure 1 Modeling of Six-barrel Multi-Capsule Water-Cooled Rod

Each of the cells in the WIMS-AECL model contains a central cell-of-interest representing an actual MCR6 lattice cell in the NRU reactor core. The central cell-of-interest is surrounded by a super-cell representing its surrounding environment of neighbouring NRU driver fuel rods, up to two pitches away. The super-cell consists of two fuel rings and an outer boron ring. The fuel rings are modeled as D_2O and U235. The boron ring is modeled as D_2O and B-10. The concentration of boron is adjusted to bring the k-effective of the cell close to 1.0 at each burnup step. D_2O fills the space between the three super-cell rings. Figure 2 presents a WIMS-AECL super-cell model for the capsule section of an MCR6 rod.

The homogenized cell parameters for the cells that represent each section of an MCR6 rod were calculated from the WIMS-AECL code. WIMS-AECL is a two-dimensional multi-group neutron transport code used for reactor lattice neutronic calculations, using the 'Pij' collision-probability method. The main transport calculations were performed using 18 energy groups, but later the cell parameters were collapsed into 2 energy groups. Examples of the cell parameters of an MCR6 rod are diffusion coefficients and various cross sections, such as absorption and removal.

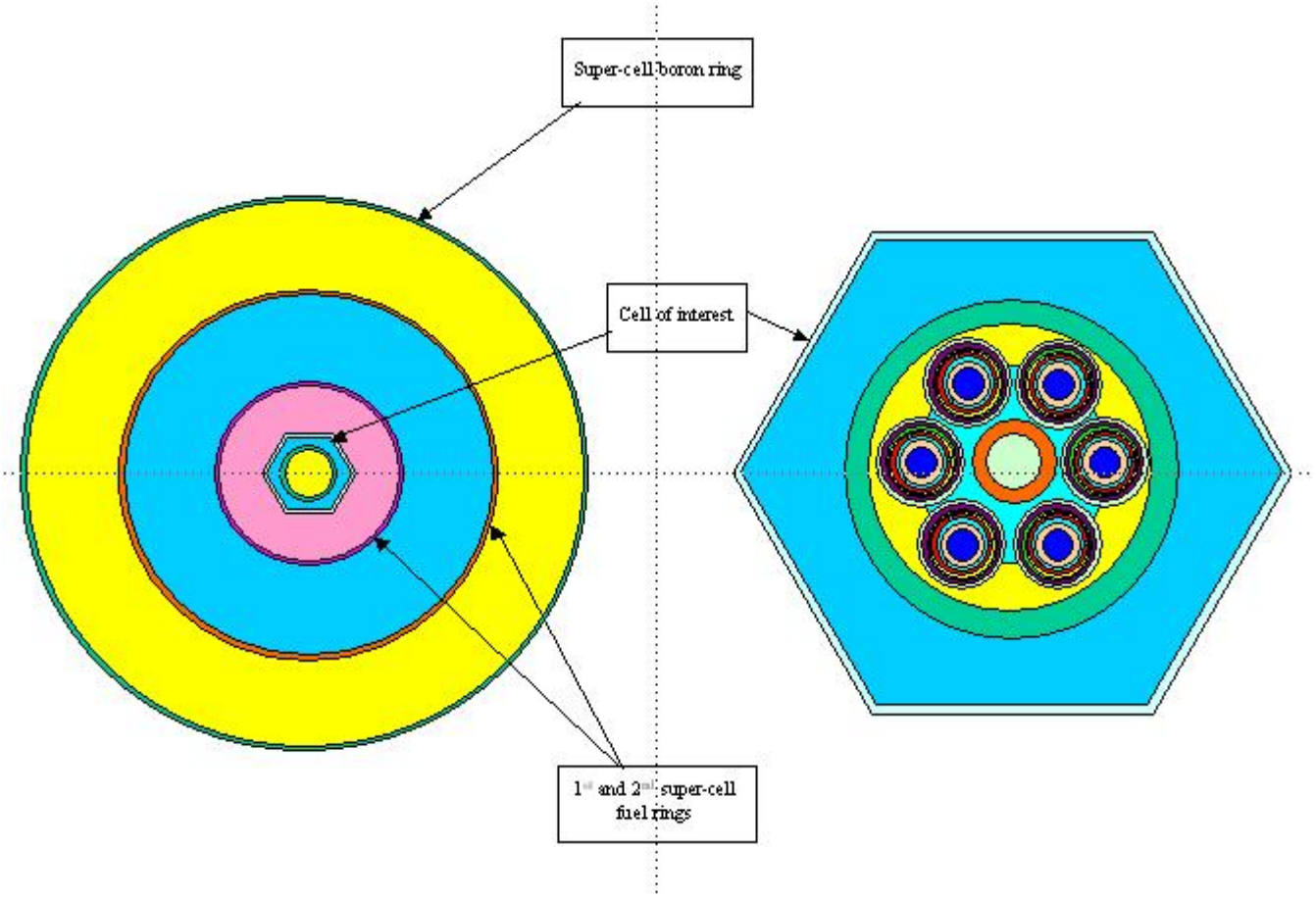

Figure 2 WIMS-AECL super-cell model of the capsule section of an MCR6 rod

This paper describes the modeling of several MCR6 rods, each with different radioisotope loadings, as listed in Table 1. The first case is the reference case of an MCR6 rod with typical loading in the middle 150 cm of the rod, in this case with TeO_2 (Irradiation of TeO_2 produces

I^{131}) in three of the six stringers and Ir (Irradiation of Iridium produces Ir^{192}) in the other three stringers. An MCR6 rod loaded with a proposed large loading of Ir (44.0 g per stringer) in the middle 150 cm of all of the six stringers (case2) was also modeled. Case 3 was an MCR6 rod with a proposed large Ir loading spread over 300 cm in each of the six stringers. The fourth case was similar to the reference case, except with Zr-Yttria material samples in one of the six stringers. The thermal neutron flux measurement was made in the MCR6 rod with this loading.

Table 1 Various loadings of an MCR rod

	Stringers	1	2	3	4	5	6
Typical Loading (case 1 as reference)	**Isotopes**	**TeO_2**	**Ir**	**TeO_2**	**Ir**	**TeO_2**	**Ir**
	Average g/stringer	1098.3	33.6	1098.3	33.6	1098.3	33.6
	Average over 150 cm (g/cm)	7.3	0.2	7.3	0.2	7.3	0.2
Proposed Large Loading Over 150 cm (case 2)	**Isotopes**	**Ir**	**Ir**	**Ir**	**Ir**	**Ir**	**Ir**
	Average g/stringer	44.0	44.0	44.0	44.0	44.0	44.0
	Average over 150 cm (g/cm)	0.3	0.3	0.3	0.3	0.3	0.3
Proposed Large Loading Over 300 cm (case 3)	**Isotopes**	**Ir**	**Ir**	**Ir**	**Ir**	**Ir**	**Ir**
	Average g/stringer	44.0	44.0	44.0	44.0	44.0	44.0
	Average over 300 cm (g/cm)	0.1	0.1	0.1	0.1	0.1	0.1
Loading With Zr-Yttria Samples (case 4)	**Isotopes**	**ZrO_2**	**Ir**	**TeO_2**	**Ir**	**TeO_2**	**Ir**
	Average g/stringer	72.0	33.6	1098.3	33.6	1098.3	33.6
	Average over 150 cm (g/cm)	2.9	0.2	7.3	0.2	7.3	0.2

2.2 TRIAD3 model for the MCR6 rod

TRIAD3 is a three-dimensional diffusion code used to calculate steady-state neutron flux and power distributions for the NRU reactor. In TRIAD3, an MCR6 rod is modeled in 18 axial sections (Sections 1 to 18, from top to bottom), each of which is represented by a WIMS-AECL lattice cell with the cell parameters generated from WIMS-AECL calculations. The 18 axial cell types for MCR6 rods with different sample loadings used in this study are listed in Table 2. The first section of each rod is the top section cell. Sections 2 to 5 and 14 to 17 are spacer section cells. The middle sections (6 to 13) are capsule section cells, and Section 18 is the bottom section cell.

Table 2 WIMS-AECL cell types in each axial section of the MCR6 rods

Axial Section No.	Axial Position Relative to the Centre of Reactor (cm)	Cell Type of an MCR6 with Typical Loading	Cell Type of an MCR6 with Large Loading over 150 cm	Cell Type of An MCR6 with Large Loading over 300 cm	Cell Type of an MCR6 with Zr-Yttria Samples
1	150.0 to 175.0	*mcr6__an*	*mcr6__an*	*mcr6__an*	*mcr6__an*
2	137.2 to150.	*mcr6__cn*	*mcr6__cn*	*mcr6llbn*	*mcr6__cn*
3	125.0 to137.2	*mcr6__cn*	*mcr6__cn*	*mcr6llbn*	*mcr6__cn*
4	100.0 to 125.0	*mcr6__cn*	*mcr6__cn*	*mcr6llbn*	*mcr6__cn*
5	75.0 to100.0	*mcr6__cn*	*mcr6__cn*	*mcr6llbn*	*mcr6__cn*
6	50.0 to 75.0	*mcr6_fbn*	*mcr6_lbn*	*mcr6llbn*	*mcr6_0bn*
7	38.0 to 50.0	*mcr6_fbn*	*mcr6_lbn*	*mcr6llbn*	*mcr6_0bn*
8	25.0 to 38.0	*mcr6_fbn*	*mcr6_lbn*	*mcr6llbn*	*mcr6_0bn*
9	0 to 25.0	*mcr6_fbn*	*mcr6_lbn*	*mcr6llbn*	*mcr6_zbn**
10	-25.0 to 0	*mcr6_fbn*	*mcr6_lbn*	*mcr6llbn*	*mcr6_0bn*
11	-38.0 to –25.0	*mcr6_fbn*	*mcr6_lbn*	*mcr6llbn*	*mcr6_0bn*
12	-50.0 to –38.0	*mcr6_fbn*	*mcr6_lbn*	*mcr6llbn*	*mcr6_0bn*
13	-75.0 to –50.0	*mcr6_fbn*	*mcr6_lbn*	*mcr6llbn*	*mcr6_0bn*
14	-100.0 to -75.0	*mcr6__cn*	*mcr6__cn*	*mcr6llbn*	*mcr6__cn*
15	-125.0 to –100.0	*mcr6__cn*	*mcr6__cn*	*mcr6llbn*	*mcr6__cn*
16	-137.2 to –125.0	*mcr6__cn*	*mcr6__cn*	*mcr6llbn*	*mcr6__cn*
17	-150.0 to –137.2	*mcr6__cn*	*mcr6__cn*	*mcr6llbn*	*mcr6__cn*
18	-175.0 to –150.0	*mcr6__dn*	*mcr6__dn*	*mcr6__dn*	*mcr6__dn*

* location of gold wire detector for thermal flux measurement

2.3 Simulation results

Neutronic simulations were performed using the TRIAD3 code for a typical NRU core with an MCR6 rod of different sample loadings installed at reactor position M17. Figure 3 shows the radial thermal neutron flux distributions across the reactor for an MCR6 rod with typical loading. The axial thermal flux distributions for an MCR6 rod with various loading at site M17 and also the neighbouring rod powers were calculated. The effects of the various loadings in the MCR6 rod on the calculation results are described below.

2.3.1 Effect of the various loadings on axial thermal flux distributions

Figure 4 shows the axial thermal flux distributions in the MCR6 rods with various loadings. For an MCR6 rod with typical loading, the flux shape is flat in the middle of the rod, which is caused by the neutron absorptions of the Ir and TeO_2 isotopes. For an MCR6 rod with a large Ir loading spread over the middle 150 cm of the rod, the flux shape is further depressed by about 30% in the middle region due to the larger amount of Ir installed there. For the rod with the large Ir loading spread over 300 cm of the rod, the flux has a distribution close to a cosine shape, but with flux reduction of about 24% in the middle region of the rod.

channel averaged cell avg thermal fluxes core 080410~b k-eff: 1.044scale = 1e+14
reactor power = 100.0 mw
Triad3PC-Power v1.1.1.1 ld=2007-02-01

burnup type: measbu lattice split: on discontinuity factors: normal

	y	z	a	b	c	d	e	f	g	h	j	k	l	m	n	o	p	q	r	s	t	
34										0.13												34
33									0.17	0.30	0.29	0.15										33
32								0.25	0.48	0.58	0.45	0.21										32
31							0.26	0.65	0.80	0.77	0.58	0.23										31
30						0.25	0.81	0.98	1.16	0.91	0.64	0.20										30
29					0.15	0.83	1.17	1.18	1.15	1.08	0.61	0.15										29
28						0.71	1.32	1.33	1.53	1.24	1.06	0.54										28
27					0.47	1.42	1.49	1.60	1.64	1.47	0.91	0.43										27
26				0.25	1.08		1.63	1.55	1.52	1.52	1.40	0.90	0.28									26
25			0.11	0.79	1.54		1.73	1.57	1.81	1.55	1.33	0.73	0.12									25
24				0.52	1.27		1.94	1.69	1.64	1.84	1.66	1.13	0.54									24
23			0.23	1.00	1.88		2.00	1.72	1.72	1.86	1.60	0.94	0.30									23
22				0.72	1.60		1.96	1.93	1.75	1.88	1.81	1.37	0.81									22
21			0.36	1.26	1.59		2.07	1.93	1.82	1.95	1.60	1.21	0.53									21
20		0.11	0.81	1.41			1.63	2.28	1.99	1.83	1.70	1.69	1.14	0.18								20
19			0.46	1.09	1.64		1.92	2.31	2.18	1.93	1.58	1.59	0.67									19
18		0.16	0.83	1.41			1.96	2.31	2.38	2.10	1.68	1.70	1.09	0.23								18
17			0.52	1.08	1.79		2.21	2.14	2.07	1.96*	1.51	1.38	0.69									17
16		0.18	0.92	1.63			2.36	2.07	2.39	2.23	1.78	1.56	1.06	0.25								16
15			0.59	1.33	2.19		2.06	2.29	2.14	2.17	1.78	1.41	0.69									15
14		0.20	1.12	2.04			2.17	2.34	2.04	2.00	2.26	1.74	1.08	0.23								14
13			0.64	1.78	2.10		2.29	2.02	1.92	2.06	1.97	1.54	0.67									13
12		0.15	1.23	1.86			2.31	2.21	1.91	1.99	2.35	2.04	1.13	0.19								12
11			0.52	1.50	2.09		2.25	1.83	1.84	2.24	2.26	1.45	0.59									11
10				0.95	2.04		2.23	1.98	1.93	1.85	2.28	1.82	0.99									10
9			0.30	1.24	2.13		2.01	1.65	1.77	1.92	2.13	1.27	0.39									9
8				0.65	1.45		2.03	1.86	1.76	1.65	2.09	1.76	0.76									8
7			0.13	0.89	1.50		1.87	1.70	1.75	1.75	1.60	1.15	0.17									7
6				0.29	1.05		1.55	1.77	1.93	1.92	1.70	1.35	0.43									6
5				0.47	1.13		1.44	1.77	1.94	1.84	1.29	0.67										5
4				0.62			1.13	1.33	1.78	1.56	1.49	0.81										4
3				0.14	0.68		1.16	1.25	1.39	1.25	0.93	0.22										3
2				0.21			0.71	0.98	1.31	1.29	0.94	0.30										2
1				0.22			0.63	0.85	0.98	0.80	0.34											1
0							0.22	0.49	0.67	0.62	0.30											0
-1								0.17	0.33	0.37	0.22											-1
-2									0.15													-2
	y	z	a	b	c	d	e	f	g	h	j	k	l	m	n	o	p	q	r	s	t	

07-NOV-08 14:59:22

1

* MCR6 rod site with gold wire detector for thermal flux measurement

Figure 3 Thermal flux distributions with a typically loaded MCR6 rod

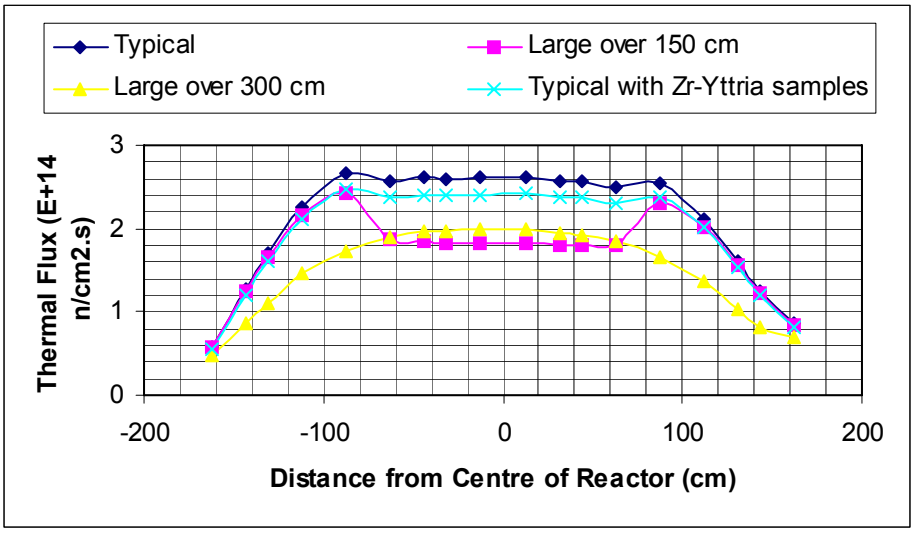

Figure 4 Axial thermal flux distributions for the MCR6 Rod at reactor position M17

2.3.2 Effect of various loadings on neighbouring rod powers

Table 3 shows the effect of the various loadings in the MCR6 rod on the thermal powers of neighboring rods. The thermal powers for both the neighboring fuel rods and Mo-99 production rods are significantly reduced for the MCR6 rod with a proposed large Ir loading as compared to the rod with a typical loading.

For the MCR6 rods with a large Ir loading spread over the middle 150 cm and 300 cm, the maximum power reductions for the neighboring fuel rods are ~20.2% and ~26.8%, respectively. The latter MCR6 rod (case 3) has a larger effect on the surrounding fuel rod powers than the former (case 2). On the other hand, for the same situation, the maximum power reductions for the neighboring Mo-99 production rods are ~27.7% and ~23.1%, respectively. The latter MCR6 rod (case 3) has a smaller effect on the Mo-99 production rod powers than the former (case 2). This is because the fuel section of the Mo-99 production rods is located in the middle ~76 cm of the rod. Since the effect of the large Ir loading on neighboring rod powers is significant, an MCR6 rod with large Ir loading (44 g Ir per string) is not recommended.

For an MCR6 rod with Zr-Yttria material samples in one of the six stringers, the effect upon the neighboring rod powers is insignificant (less than 0.9%).

Table 3 Powers of fuel sites and Mo99 sites adjacent to the MCR6 rod at M17

		Typical Loading (MW)	Large Loading Over 150 cm (MW)	Large Loading Over 300 cm (MW)	Loading with Zr-Yttria Samples (MW)
Fuel Sites	K17	1.538	1.421 (-7.61%)*	1.311 (-14.76%)*	1.530 (-0.53%)*
	L14	1.411	1.206 (-14.53%)*	1.103 (-21.83%)*	1.404 (-0.50%)*
	N16	1.138	0.908 (-20.21%)*	0.833 (-26.80%)*	1.134 (-0.35%)*
	N18	0.599	0.543 (-9.35%)*	0.497 (-17.03%)*	0.596 (-0.50%)*
Mo99 Sites	M15	0.242	0.175 (-27.69%)*	0.186 (-23.14%)*	0.240 (-0.83%)*
	L18	0.233	0.202 (-13.3%)*	0.213 (-8.58%)*	0.232 (-0.43%)*

* The values in the parentheses are the percent changes in rod powers with respect to the reference case (an MCR6 rod with typical loading).

3. Thermal flux measurement in the MCR6 rod

3.1 Measurement method

The thermal neutron flux in the MCR6 rod at reactor position M17 was determined by the neutron activation method using gold wires. Two gold wires, each of 1.0 mm in diameter and 5.0 cm long, were put in two capsules near the center of the reactor in the stringer with Zr-Yttria material samples. The gold wires were irradiated from 2008 April 5 to 20, with one reactor shutdown during this period. During the irradiation, the Au-197 nuclides of the gold

wire formed new isotopes of Au-198 as neutrons were absorbed. The Au-198 isotope is unstable, and decayed as well being removed by neutron capture.

$$Au^{197} + n \rightarrow Au^{198} \xrightarrow{\beta} Hg^{198} + \gamma(411kev) \qquad (1)$$

The build-up of the new nuclei of Au-198 in a neutron flux at any time, t, is given by

$$N_2(t) = \frac{N_1 \sigma_{a1} \phi_a}{\lambda_{2T}} (1 - \exp(-\lambda_{2T} t)) + N_2(0) * \exp(-\lambda_{2T} t) \qquad (2)$$

where N_1 and N_2 are the number densities of the Au-197, and newly formed nuclides, Au-198, respectively,

ϕ_a is the average thermal flux absorbed by the gold wire during the irradiation period,

λ_2 is the probability of radioactive decay of Au-198,

σ_{a1} and σ_{a2} are the microscopic absorption cross sections of Au-197, and Au-198, respectively, and

λ_{2T} is the effective probability, which is the sum of λ_2 and $\sigma_{a2}\phi_a$.

In this study, the NRU flux is assumed to be very well thermalized, and the resonance flux is small compared to the thermal flux. It is also assumed that the self-shielding correction is small for the thin gold wire. The gold wire microscopic absorption cross sections in Eq. (2), σ_{a1} and σ_{a2}, are the average cross sections over a Maxwellian distribution for temperature in degrees Kelvin, T. $\sigma_a = \sigma_{a,2200}(\sqrt{\pi}/2)(T_0/T)^{1/2}$, where $\sigma_{a,2200}$ = cross section at a neutron speed of 2200 m/s, which is corresponding to Maxwellian flux distribution at 20.46 ^{0}C (293.61K). The $\sigma_{a1,2200}$ and $\sigma_{a2,2200}$ are taken to be 98.7 and 2600 barns, respectively [5]. For the gold wire that was un-irradiated initially, $N_2(0) = 0$, at $t = 0$. When the gold wire was removed from the reactor, it decayed with its own characteristic half-life, $(T_{1/2})_2$. Its activity was $\lambda_2 N_2$, where $\lambda_2 = \ln 2/(T_{1/2})_2$. From the measured activities of Au-198, $\lambda_2 N_2$, the average neutron flux seen by the gold wire, ϕ_a, can be determined by Eq. 2 using a systematic trial and error method.

3.2 Flux measurement results

The two irradiated gold wires were taken out of the NRU reactor at 22:00 h on 2008 April 20. Because of the high activity, the wires were not counted until 2008 June 10. The 411.8 keV gamma peaks from the Au-198 nuclides were counted with an efficiency of 0.0695%, using a high purity Germanium (HPGe) detector. The activities of the Au-198 nuclides in the two wires, were decay corrected to the end of the irradiation period, 2008 April 20, 2200 h, and they were both found to be the same, (1.90 $\pm$0.04) x10^{13} Bq/g of wire. Then, Eq. 2 was used to determine the neutron fluxes absorbed by the gold wire, ϕ_a , during the irradiation period.

The value of ϕ_a was determined by the method of systematic trial and error to be (1.69 $\pm$ 3%) x 10^{14} n.cm^{-2}.s^{-1}.

After correcting for the absorbing probability of the gold wire, the measured neutron flux at the detector location was 1.33 times the average neutron flux seen by the gold wire, and was equal to 1.33 x 1.69 = (2.25 $\pm$ 4%) x 10^{14} n.cm^{-2}.s^{-1} (see Appendix A [6]).

3.3 Comparison of measured flux with simulations

Results of the flux simulation from the TRIAD3 code at the axial cell containing the gold wire during the irradiation period were shown in Table 4. The simulated cell-averaged fluxes and the fluxes at the detector located are listed in column 2 and 3 of the table, respectively, both normalized to the NRU reactor power of 100 MW. As discussed in the previous section, the ratio of the flux at detector location over the cell-average flux was assumed to be constant during the irradiation period, and from the result of the WIMS-AECL calculation, it was 0.829 $\pm$ 1 %. The average simulated flux at the detector wire location over the irradiation period was (1.994 $\pm$ 4 %) x 10^{14} n.cm^{-2}.s^{-1}.

During the irradiation period, the average operating power of NRU was determined by dividing the change in TPD (total power developed by the NRU reactor) by the irradiation time, and this was equal to (1037060.3-1035463.7) MWdays / 13.95 days, or 114.45 MW.

The simulated flux at the detector wire location at the averaged NRU operating power of 114.45 MW during the irradiation was thus 1.994 x (114.45/100.00)= (2.282 $\pm$ 4 %) x 10^{14}

n.cm^{-2}.s^{-1}.

Table 4 Results of the simulated fluxes during the irradiation period

Cores/date (yyyy/mm/dd)	TRIAD3(IRR) Cell Average Flux for NRU at 100 MW (x 10^{14} n.cm^{-2}.s^{-1})	Simulated Flux at Detector Wire Location for NRU At 100 MW *x 0.829$\pm$ 1%* (x 10^{14} n.cm^{-2}.s^{-1})	Simulated Flux at Detector Wire Location for NRU at 114.45 MW (x 10^{14} n.cm^{-2}.s^{-1})
2008/04/10	2.421 $\pm$ 3 %	2.007 $\pm$ 4 %	---
2008/04/11	2.464 $\pm$ 3 %	2.042 $\pm$ 4 %	---
2008/04/13	2.446 $\pm$ 3 %	2.028 $\pm$ 4 %	---
2008/04/15	2.311 $\pm$ 3 %	1.916 $\pm$ 4 %	---
2008/04/16	2.387 $\pm$ 3 %	1.979 $\pm$ 4 %	---
Average Flux =		1.994$\pm$ 4 %	2.282 $\pm$ 4 %

From the results of the last two sections, the measured-to-simulated flux ratio at the detector wire location was (2.25 $\pm$ 4 % /2.28 $\pm$ 4 %)=0.98. This indicates that the simulated flux over-predicted the flux at the detector location by ~ 2%. The agreement between the measured and simulated values of the fluxes is exceedingly good and this is within the combined uncertainty of the measured and simulated fluxes, which is expected to be about $\pm$ 8 %.

4. Conclusions

The NRU MCR6 rods with various loadings in the stringers have been modeled. Sensitivity studies of the neutronic simulations on flux distributions in the MCR6 rods and the powers of the neighboring rods have been performed. The thermal fluxes in the MCR6 rod with Zr-Yttria material samples in one of the six stringers were measured and compared with the simulation fluxes.

The main conclusions drawn in this study are

1. Results of neutronic simulations with the TRIAD3 code for a typical NRU core show a thermal flux reduction of up to ~30% in the middle region of the MCR6 rods and power reductions of up to ~27 % at sites neighboring MCR6 rods with 44g Ir per string.

2. The measured thermal flux in the MCR6 rod is in good agreement with the simulated flux (within 2%).

3. The gold wire flux measurement data confirmed that the model of the MCR6 rod used in the TRIAD3 code is correct within the expected accuracy.

5. References

[1] D.T. Nishimura, "Summary of loops in Chalk River NRX and NRU reactors", AECL report, AECL-6980, 1980 December.

[2] J. D. Irish and S.R. Douglas, "Validation of WIMS-IST", Proceedings of 23rd Annual Conference of the Canadian Nuclear Society, Toronto, Canada, 2002 June.

[3] S. R. Douglas, "A calculational model for the NRU reactor", Paper presented at the Canadian Nuclear Society 1985 Annual Conference, 1985 June.

[4] J. Chang, M. Bates and etc., "The ACR-1000 Fuel Bundle Technical Specifications", 10th International Conference on CANDU Fuel, Ottawa, Canada, 2008 October.

[5] E. M. Baum, H.D. Knox and T.R. Miller, "Chart of the nuclides", Knolls Atomic Power Laboratory, U.S. Department of Energy, Sixteenth Edition, 2002.

[6] K. H. Beckurts and K. Wirtz, "Neutron Physics", Published by Springer-Verlag, 1964.

Appendix A: Flux Correction for the Absorption Probability of a Thin Cylindrical Wire [6]

For a number of neutrons incident on a thin cylindrical wire, only a fraction of the neutrons are absorbed. If the number of radioactive atoms formed by neutron capture per second per 1 cm length of wire is C, then

$$C = (\pi R \bar{\phi}_{mea} / 2) * \chi_0(\Sigma_a R), \quad \text{(A.1)}$$

Where $\bar{\phi}_{mea}$ is the measured thermal neutron flux at the detector wire location, averaged over the irradiation period,

R is the radius of the wire, and

$\pi R(\bar{\phi}_{mea})/2$ is the number of neutron incident per second on the cylindrical surface of 1 cm of the wire, and $\chi_0(\Sigma_a R)$ is the absorption probability of neutrons with an isotropic distribution of velocity incident on the 1 cm length of wire.

The detailed calculation for the absorption probability for a thin cylindrical thin wire, $\chi_0(\Sigma_a R)$, is given in reference 5. The value of $\chi_0(\Sigma_a R)$ as a function of $\Sigma_a R$ is shown in Figure A-1. The function approaches unity for large values of $\Sigma_a R$, but for thin cylinders, $\chi_0(\Sigma_a R) \approx 2\Sigma_a R$.

In addition, the number of Au-198 radioactive nuclides formed in a volume of 1 cm length of cylindrical wire is

$$C = \pi R^2 \Sigma_a \phi_a, \quad \text{(A.2)}$$

where ϕ_a is the neutron flux absorbed by the gold wire.

Therefore, combining Eqs. (A.1) and (A.2):

$$\bar{\phi}_{mea} = \left(\frac{2\Sigma_a R}{\chi_0}\right) * \phi_a \quad \text{(A.3)}$$

For the irradiated gold wire of 1.00 mm diameter in our study, the value of $\Sigma_a R$ was 0.250, and from Figure A-1, the calculated value of $\chi_0(\Sigma_a R)$ was 0.377. Therefore,

$$\bar{\phi}_{mea} = 1.33\phi_a \quad \text{(A.4)}$$

The measured neutron flux at detector gold wire location, $\bar{\phi}_{mea}$, is 1.33 times the flux absorbed by the thin wire, ϕ_a.

Figure A-1 The absorption probability, $\chi_0(\Sigma_a R)$, of a thin cylindrical wire [6]